Decoupling Between Extremely Closely Spaced Patch Antennas by Mode Cancellation Method

Libin Sun, *Graduate Student Member, IEEE*, Yue Li, *Senior Member, IEEE*, and Zhijun Zhang, *Fellow, IEEE*

***Abstract*— In this article, an inductance-based decoupling scheme is proposed to reduce the mutual coupling between extremely closely spaced microstrip antennas. The original strong coupling can be effectively suppressed by simply inserting a lumped inductance in between. To offer a systemic design guideline for this decoupling strategy, a mode cancellation method, based on the synthesis of common mode (CM) and differential mode (DM), is proposed. The inserted inductance plays a role of tuning CM and DM impedances to a similar status, which has an equivalent decoupling effect according to the theory of microwave network. Alternatively, the lumped inductance could also be replaced by an inductive connecting strip for a concise topology. To validate the proposed decoupling concept, a prototype is simulated, fabricated, and measured. The experimental results show that the poor isolation of 5 dB is improved to better than 15.4 dB across the entire matched bandwidth of 2.394–2.530 GHz, with an extremely close edge-to-edge distance of 0.016 λ_0 and center-to-center distance of 0.44 λ_0. Furthermore, the validation of extending to large-scale 1-D and 2-D arrays is also discussed. Featuring simple structure, compressed dimension, strong-coupling suppression, and good radiation performance, the proposed decoupling scheme possesses promising potential for antenna array applications.**

***Index Terms*— Closely spaced patch antennas, decoupling, mode cancellation method (MCM), multiple-input multiple-output (MIMO), mutual coupling.**

I. Introduction

IN RICH multipath environments, the channel capacity of wireless communication systems can be improved drastically by employing multiple-input and multiple-out (MIMO) technology, at no additional expense in spectrum or power resources [1]–[3]. Given these benefits, MIMO technology has attracted considerable attention in academic and industrial communities and has been widely implemented in up-to-date wireless communication systems. However, in the size-limited terminal or portable devices, the closely spaced antenna elements arrangement will lead to a high mutual coupling or correlation coefficient between antenna elements, thus degrades the MIMO performance. To address this issue, plenty of researches have been focused on mitigating the mutual coupling between closely spaced antenna elements to realize a high isolation and a satisfactory MIMO performance [4]–[38].

In general, there are three different techniques to reduce the mutual coupling between same-polarized antenna elements in the open literature [4], [5].

The *first* decoupling scheme is decoupling network [6]–[10], which is realized by the combination of decoupling and matching networks by performing the scatter or impedance matrix operations. This scheme makes a systemic and mathematic analysis of the scatter parameters; however, the circuit-level decoupling method cannot offer an intuitive insight of the antenna radiation performance.

The *second* decoupling technique is blocking the surface current between antenna elements by band-stop structures, such as electromagnetic bandgap (EBG) [11]–[13], soft surface [14], and detected ground structures (DGSs) [15]–[20]. The EBG and soft surface provide conspicuous decoupling effect, but suffer from complex structure and large occupied dimension, which is not appropriate for the closely spaced configuration. The DGS is originated from N pairs of etched slits in the ground plane with a large implementation space [15], [16], but soon developed to a single quarter-wavelength [17], [18] or half-wavelength [19] resonant slot with a compact footprint to block the surface wave effectively; however, the etched resonant slot will generate extra backward radiation, thereby deteriorating the radiation performance.

The *third* decoupling method is canceling the original coupling by adding an extra coupling path with equal amplitude but out of phase. The specific structures of this method can be neutralization lines (NLs) [21]–[27], parasitic elements [28]–[35], and self-decoupled elements [36]–[38]. The NL and parasitic elements have the ability to perform a coupling suppression between antenna elements by an extra decoupling structure. The self-decoupled elements can reduce the mutual coupling by well-designed antenna elements instead of using extra decoupling structure, which possess ingenious antenna structures but lack systemic design guidelines and only stay at try-and-error stage so far.

Great efforts have been made to reduce the mutual coupling between microstrip antennas in the last decades [10]–[14], [16], [19], [23], [30], [34], [35]; however, most of the previous work suffer from complex decoupling structure, narrow decoupling bandwidth, and

Manuscript received October 19, 2019; revised June 16, 2020; accepted October 6, 2020. Date of publication October 20, 2020; date of current version June 2, 2021. This work was supported in part by the National Natural Science Foundation of China under Contract 61971254 and Contract 61525104, and in part by the Beijing Natural Science Foundation under Contract 4182029. *(Corresponding author: Zhijun Zhang.)*

The authors are with the Beijing National Research Center for Information Science and Technology (BNRist), Tsinghua University, Beijing 100084, China (e-mail: zjzh@tsinghua.edu.cn).

Color versions of one or more of the figures in this article are available online at https://ieeexplore.ieee.org.

Digital Object Identifier 10.1109/TAP.2020.3030922

degraded radiation pattern when in the closely spaced array configuration. To tackle these technical hurdles, a simple and effective approach is proposed to reduce the mutual coupling between strongly coupled patch antennas, as well as keep a sufficient bandwidth and an improved radiation performance. By inserting a lumped inductance between two extremely closely spaced patch antennas, the original poor isolation of 5 dB can be improved to better than 15.4 dB across the entire matched band of 2.394–2.530 GHz. Moreover, the radiation pattern is improved to symmetric beam, high broadside gain, high front–back ratio (FBR), and low cross-polarization, even in the extremely closely spaced arrangement. To explicate the operating mechanism of the proposed decoupling scheme, a mode cancellation method (MCM) [39], based on the synthesis of common mode (CM) and differential mode (DM), is presented to provide a systemic design guideline. Compared to the previous decoupling approaches, the proposed decoupling scheme features simple structure, compressed dimension, strong-coupling suppression, moderate bandwidth, and improved radiation performance.

This article is organized as follows. In Section II, the design guideline of the proposed inductance-based decoupling scheme with some design cases is proposed based on the MCM. In Section III, a practical design example is simulated, fabricated, and measured to validate the proposed decoupling scheme, and a comparison table is also presented to highlight the merits. In Section IV, the validation of extending to large-scale 1-D and 2-D arrays is discussed. Finally, Section V draws a conclusion.

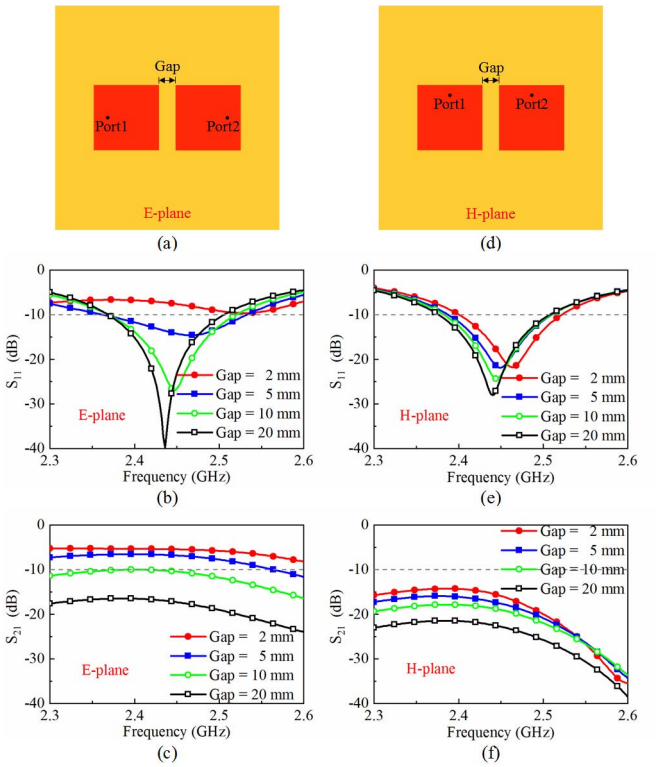

Fig. 1. Configurations of the E- and H-planes arrayed dual-element patch antennas and the corresponding simulated S-parameters (the patch antennas are modeled in the air medium with a profile of 0.04 λ_0). (a) E-plane arrayed patch antennas and (b) simulated S_{11} and (c) simulated S_{21} with the element distance varied. (d) H-plane arrayed patch antennas and (e) simulated S_{11} and (f) simulated S_{21} with the element distance varied.

II. Design Guideline

A. E-Plane and H-Plane Element Arrangement

In general, there are two different array configurations for patch antennas: E-plane and H-plane array configurations, the isolation of which have a huge discrepancy. Fig. 1 shows the sketch diagram of the E-plane and H-plane arrayed patch antennas and the corresponding S-parameters with the edge-to-edge distance varied. Note that the patch antennas are modeled in the air medium with a low profile of 0.04 λ_0. For the E-plane arrangement, the impedance matching and isolation are severely influenced by the decrease of the element distance, as shown in Fig. 1(b) and (c). When the element distance is reduced to 2 mm (0.016 λ_0), the S_{11} is deteriorated to worse than -10 dB and the isolation is only about 5 dB. However, for the H-plane arrangement, the impedance matching and isolation are only slightly affected by the element distance as shown in Fig. 1(e) and (f). The radiation edges of two patch antennas are adjacent for the E-plane array whereas the nonradiation edges are adjacent for the H-plane array, which contributes to the large isolation discrepancy between E-plane and H-plane arrays. Note that this conclusion is not applicable for the planar patch antenna with a thick dielectric substrate, which has a strong surface-wave coupling effect instead of spatial field coupling only [34]. Since the isolation of closely spaced H-plane array is satisfactory in the air medium, so we mainly focus on the decoupling between closely spaced E-plane array in this article.

B. Decoupling Mechanism

According to the theory of microwave network [40], [41], a symmetric ($S_{11} = S_{22}$) and reciprocal ($S_{21} = S_{12}$) single-ended 2-port network can be transformed to a CM/DM network and satisfies the S-parameters relation of

$$S_{cc11} = (S_{11} + S_{12} + S_{21} + S_{22})/2 = S_{11} + S_{21} \quad (1)$$

$$S_{dd11} = (S_{11} - S_{12} - S_{21} + S_{22})/2 = S_{11} - S_{21}. \quad (2)$$

Combined with (1) and (2), we have

$$|S_{cc11} - S_{dd11}| = 2|S_{21}|. \quad (3)$$

Therefore, the perfect isolation condition ($S_{21} = 0$) in the single-ended 2-port network can be transformed to $S_{cc11} = S_{dd11}$ in the CM/DM network. And a better isolation can be achieved with a more similar CM and DM S-parameters. In other words, the decoupling problem between two symmetrical antenna elements can be equivalent to tuning the corresponding CM and DM impedances to be consistent, which offers a new insight for the antenna decoupling.

To provide an intuitive insight of the aforementioned concept, the E-field distributions of CM and DM are demonstrated in Fig. 2(a) and (b), respectively. If two patch elements are simultaneously excited with in-phase signal, a combined TM_{20} mode (CM) is realized as shown in Fig. 2(a). On the contrary, if two patch elements are simultaneously excited with out-of-phase signal, a combined antiphase TM_{20} mode (DM) is

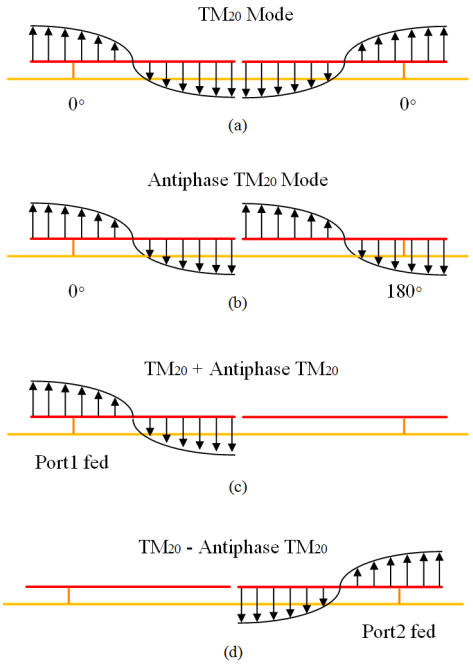

Fig. 2. E-field distributions in (a) CM excitation, (b) DM excitation, (c) port1 excitation, and (d) port2 excitation.

realized as shown in Fig. 2(b). When the TM_{20} mode and antiphase TM_{20} mode are superposed with equal amplitude and phase, as illustrated in Fig. 2(c), the E-field in the left patch element is enhanced while that in the right patch element is canceled. If we have the condition of $S_{cc11} = S_{dd11}$, the CM and DM feeding sources can be superposed in the same way with the feeding signal in port2 canceled. Therefore, an isolated E-field distribution can be realized when fed through port1. Similarly, as shown in Fig. 2(d), an isolated E-field distribution can also be realized in the second patch element when fed through port2 by the subtraction of TM_{20} and antiphase TM_{20} modes.

C. Decoupling Between Two Closely Spaced E-Plane Patch Antennas With Symmetric Ports Configuration

Fig. 3 shows the array configuration of two extremely closely spaced E-plane arrayed patch antennas with symmetric ports configuration. Two square patch elements (in red), with a dimension of 58 × 58 mm^2, both operate at the TM_{01} mode. The patch elements are installed in the air substrate with a low profile of Hp = 5 mm above a 200 × 200 mm^2 ground plane (in yellow). The edge-to-edge distance is 2 mm ($0.016\lambda_0$) with a strong original coupling of 5 dB as early shown in Fig. 1(c).

According to the theory in Section II-B, we can exploit CM and DM impedances to analyze and mitigate the mutual coupling of the proposed 2-element patch array. For CM, as shown in Fig. 4(a), the symmetric plane is equivalent to a perfect magnetic conductor (PMC) with an open-circuit condition [42]. For DM, as shown in Fig. 4(b), the symmetric plane is equivalent to a perfect electric conductor (PEC) with a short-circuit condition, in which case the patch edges will bring a coupling capacitance effect [42]. The different

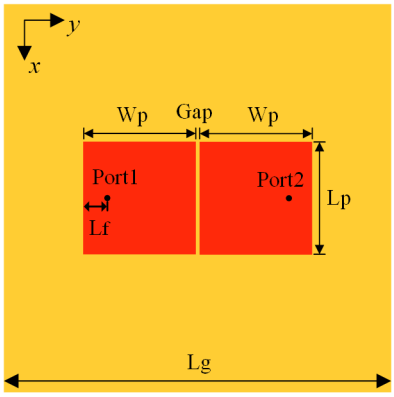

Fig. 3. Configuration of the extremely closely spaced E-plane patch antennas with symmetric ports configuration. Detailed dimensions: Lg = 200 mm, Lp = 58 mm, Wp = 58 mm, Lf = 12 mm, and Gap = 2 mm.

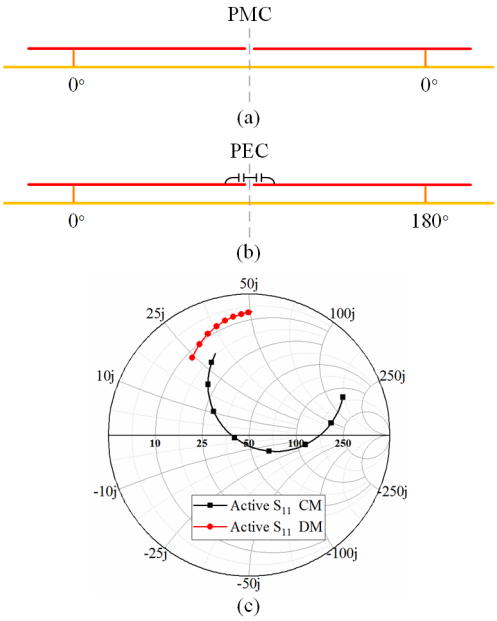

Fig. 4. (a) Equivalent boundary condition in the CM feed. (b) Equivalent boundary condition in the DM feed. (c) Simulated Smith chart of the active S_{11} for CM and DM (frequency spans: 2.3–2.6 GHz).

boundary conditions in the symmetric plane lead to the different impedances for CM and DM, as shown in Fig. 4(c), which means poor isolation between two patch elements.

To achieve a similar impedance for CM and DM, a feasible solution is altering the DM center boundary condition from PEC to PMC, while the CM center boundary condition keeps open-circuit unchanged. Undoubtedly, an effective solution is to create a parallel LC resonator. If an inductance is inserted between two patch elements, the center boundary condition of CM is not affected due to the open-circuit response, as shown in Fig. 5(a), while that of DM is changed because the inserted inductance can be combined with the coupling capacitance to create a parallel LC resonator as shown in Fig. 5(b). And the parallel LC resonator exhibits an open-circuit impedance response at the resonant frequency f_0 [40]

$$f_0 = \frac{1}{2\pi\sqrt{LC_g/2}} \tag{4}$$

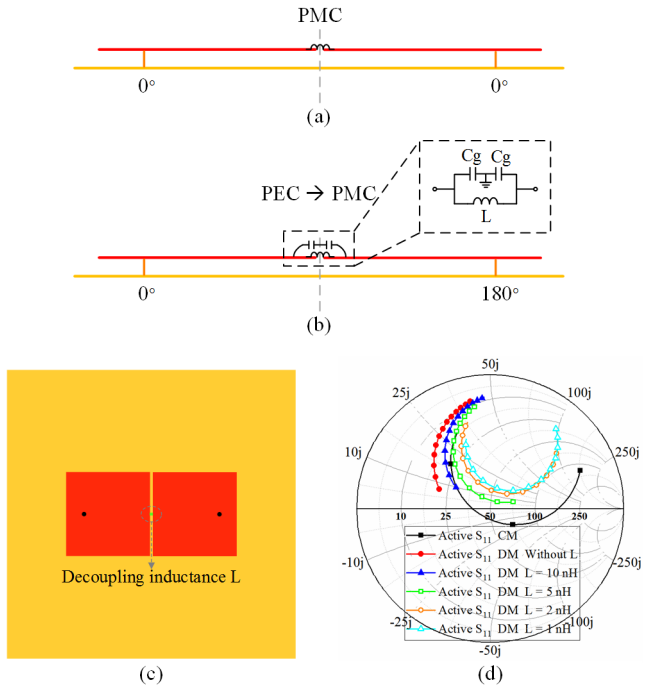

Fig. 5. (a) Equivalent boundary condition of the CM feed with an inserted inductance. (b) Equivalent boundary condition of the DM feed with an inserted inductance, inset shows the equivalent circuit. (c) Antenna model with the decoupling inductance inserted. (d) Simulated Smith chart of the active S_{11} for CM and DM with the inductance value varied (frequency spans: 2.3–2.6 GHz).

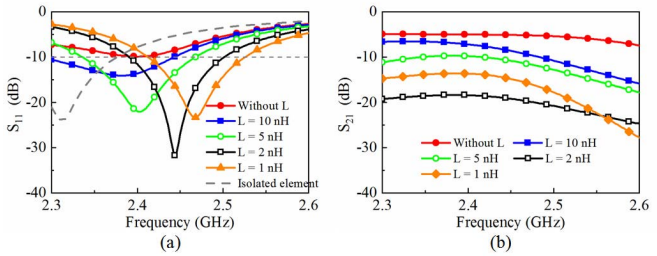

Fig. 6. (a) Simulated single-ended S_{11} and (b) simulated S_{21} with the decoupling inductance L varied.

where C_g is the unilateral coupling capacitance between two coupled microstrip antennas. Therefore, by inserting an inductance that satisfies (4) between two extremely closely spaced patch antennas, as shown in Fig. 5(c), the DM impedance can be tuned to a similar status to the CM impedance. Fig. 5(d) shows the active S-parameters of CM and DM with the inserted inductance L varied. As seen, with the decrease of L, the DM active S-parameter is close to the CM active S-parameter gradually, and an optimized similarity is achieved when $L = 2$ nH; meanwhile, the CM active S-parameter keeps unchanged with the variation of L, which is not shown for brevity.

The single-ended S_{11} and S_{21} with the decoupling inductance L varied are presented in Fig. 6(a) and (b), respectively. As seen, both the impedance matching and isolation are improved with the insertion of the decoupling inductance.

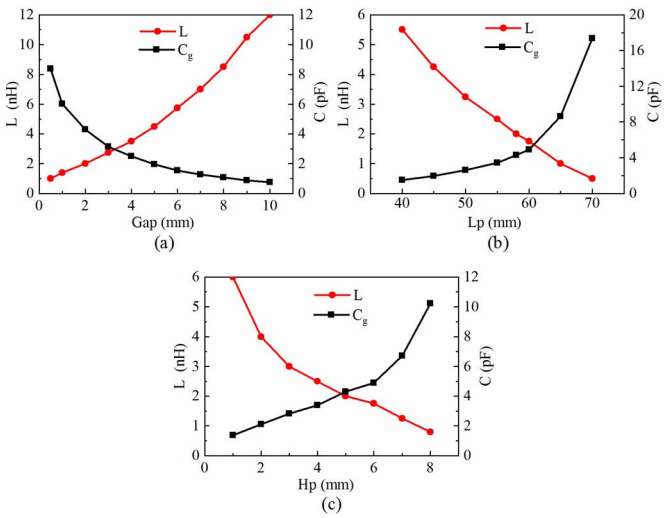

Fig. 7. Simulated optimized decoupling inductance L and the corresponding coupling capacitance Cg with the variations of (a) element distance Gap, (b) patch length Lp, and (c) patch height Hp.

The isolation reaches to an optimized value of better than 18.4 dB when $L = 2$ nH. At the same time, a good impedance matching is realized with a deep resonance and a -10 dB bandwidth of 2.39–2.50 GHz. Consequently, the strong coupling between extremely closely spaced patch antennas is mitigated and the impedance matching is improved by simply inserting an inductance.

To offer an empirical design rule when the antenna sizes are altered, the simulated results of the optimized decoupling inductance L and the corresponding coupling capacitance C_g with the variations of Gap, Lp, and Hp are proposed in Fig. 7. Note that the coupling capacitance is derived by the optimized inductance and resonant frequency according to (4). As shown in Fig. 7(a), the coupling capacitance is decreased and the optimized decoupling inductance is increased with the increasing of the element distance Gap. On the contrary, the coupling capacitance is increased and the decoupling inductance is decreased with the increasing of the patch length Lg and patch height Hg, as shown in Fig. 7(b) and (c), respectively.

The current and *E*-field distributions with and without the inserted inductance are demonstrated in Fig. 8 for an intuitive comparison. Without the inserted decoupling inductance, as shown in Fig. 8(a) and (c), the closely spaced array arrangement leads to a strong *E*-field coupling between adjacent patch elements. However, after inserting a 2 nH inductance, as shown in Fig. 8(b) and (d), the mutual coupling is obviously blocked with most of the field bounded in the left patch element when fed through port1.

With the blocked *E*-field distribution, the far-field radiation performance can be improved accordingly as shown in Fig. 9. Without the decoupling inductance, the strong coupling makes a beam splitting and severe gain drop in the far-field radiation pattern. With the help of the decoupling inductance, the radiation patterns in both E- and H-planes can be obviously improved to achieve a high broadside gain of 8.9 dBi, a high FBR of 25 dB, and a symmetric-shaped radiation pattern.

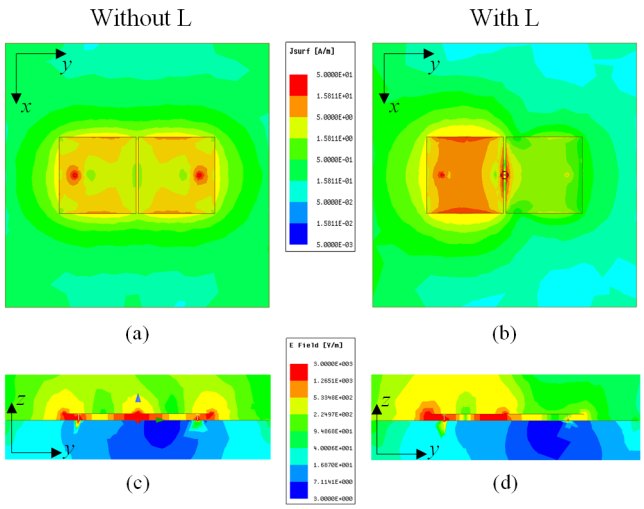

Fig. 8. Current distributions in *xy* plane fed through port1 (a) without and (b) with the inserted decoupling inductance. *E*-field distributions in *yz* plane fed through port1 (c) without and (d) with the inserted decoupling inductance.

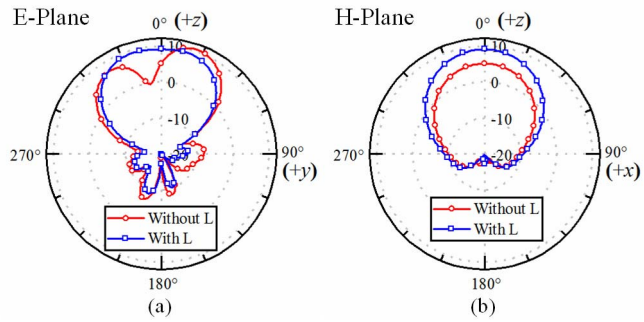

Fig. 9. Simulated radiation pattern without and with the decoupling inductance L when fed through port1 in (a) E- and (b) H-planes.

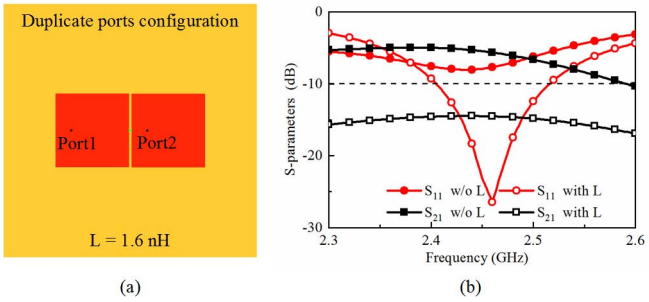

Fig. 10. (a) Configuration of the extremely closely spaced E-plane patch antennas with duplicate ports configuration. (b) Corresponding simulated S-parameters with and without the decoupling inductance.

D. Decoupling Between Two Closely Spaced E-plane Patch Antennas With Duplicate Ports Configuration

In addition to symmetric ports configuration, the proposed decoupling technology is also applicable for closely spaced patch antennas with duplicate ports configuration, which can be further extended to a large-scale array. A design case of duplicate ports configuration is proposed in Fig. 10. Note that the antenna dimension is the same as that in the symmetric ports configuration in Fig. 3, while the value of the decoupling inductance is optimized to 1.6 nH. As seen, both of the impedance matching and isolation are improved with the insertion of the decoupling inductance. However, compared to the symmetric ports configuration with an optimized isolation of better than 18.4 dB, the duplicate ports configuration shows a slight performance decline with an optimized isolation of better than 14.5 dB.

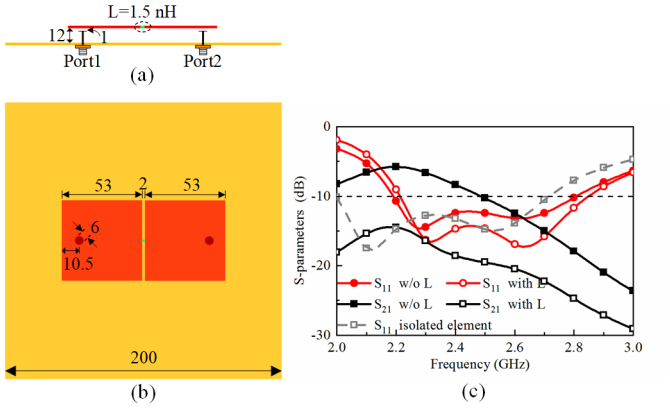

Fig. 11. Configuration of the extremely closely spaced patch antennas with a higher profile of 0.1 λ_0 and coupling-fed technology for the bandwidth enhancement. (a) Side view. (b) Top view. (c) Simulated S-parameters with and without the decoupling inductance. Unit all in millimeter.

E. Bandwidth Enhancement

In the above design cases, the achieved decoupling and matching bandwidth is about 5%, which may be limited in some practical applications with a broadband requirement. Here, a bandwidth enhancement design case for the proposed inductance-based decoupling technology is proposed. The matching bandwidth of the decoupled antenna mainly depends on the original bandwidth of the patch element. Instead, the decoupling bandwidth is not limited for this decoupling technology even in the extremely closely spaced configuration. Therefore, the matching and decoupling bandwidth of the proposed 2-element array can be readily enhanced by a wider element bandwidth. As we all known, the bandwidth of patch antennas can be improved by the high profile, coupling-fed technology, parasitic resonance, and multimode technology. As shown in Fig. 11(a) and (b), a higher profile of 12 mm (0.1 λ_0) and capacitive coupling-fed technology are used to increase the impedance bandwidth of the isolated patch element to 30.5%. And an inductance with an optimized value of 1.5 nH is inserted in-between for the coupling reduction. The simulated S-parameters with and without the decoupling inductance is shown in Fig. 11(c). As seen, a wide matched bandwidth of 2.21–2.85 GHz (25.6%) is realized. Across the matched bandwidth, the isolation is improved from 5.8 to 14.6 dB by the proposed decoupling technology.

III. Design Example

A. Practical Antenna Model

To demonstrate the proposed inductance-based decoupling scheme, a practical antenna model is simulated, fabricated,

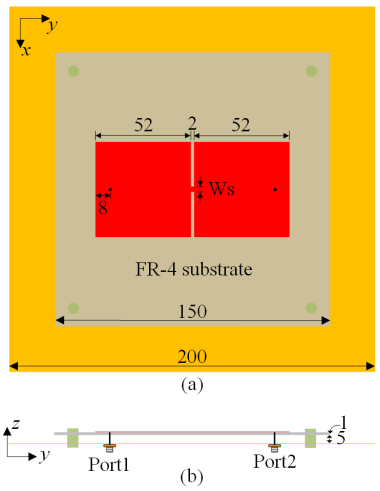

Fig. 12. Model of the practical extremely closely spaced patch antennas with a center connecting strip for decoupling. (a) Top view. (b) Side view. Unit all in millimeter.

and measured. As shown in Fig. 12, the patch elements are printed on the top layer of a 1 mm thick FR-4 substrate ($\varepsilon_r = 4.4$, $\tan\delta = 0.02$) for ease of fabrication and fixing. The FR-4 substrate is fixed by four nylon pillars with an air gap of 5 mm above the bottom ground plane. The patch size and feeding position are slightly modified compared to that in Fig. 3 due to the impact of the FR-4 substrate. Furthermore, with the increase of the equivalent permittivity, the coupling capacitance between two patch elements is significantly enhanced. Therefore, the decoupling inductance should be decreased accordingly to keep the *LC* resonant frequency unchanged. The final optimized value of the decoupling inductance is decreased to 0.04 nH, which is an infeasible value for any practical chip inductance. Alternatively, the tiny inductance can be substituted by a short connecting strip, which has an inherent inductive effect. Compared to the lumped inductance, the short strip has the merits of low cost, low loss, and continuous tuning ability. The final geometry with a short connecting strip in between is shown in Fig. 12. The center short strip connects the left and right patch elements to shape a holonomic dumbbell-like structure, which shows an equal decoupling ability with the lumped inductance. It should be noted that the proposed decoupling technology is different from the NL technology [21]–[27] although the same connecting strip is used. The principle of the proposed decoupling technology is to block the coupling field through introducing a parallel *LC* resonance via an inserted lumped or distributed inductance, which is different from the coupling cancellation effect of the NL technology.

B. Parameter Analysis

The length and width of the connecting strip will affect the equivalent inductance value, thus impacts the element isolation. In our design, the length of the connecting strip is fixed by the edge-to-edge distance to 2 mm, so the width Ws is a critical parameter to tune the isolation between two patch elements. The S_{11} and S_{21} curves with the strip width Ws varied is shown in Fig. 13(a) and (b), respectively. As seen, both the resonant frequency and isolation can be tuned by Ws.

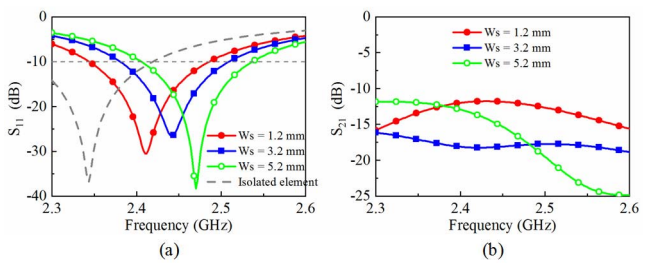

Fig. 13. Simulated (a) S_{11} and (b) S_{21} with the width of the center connecting strip Ws varied.

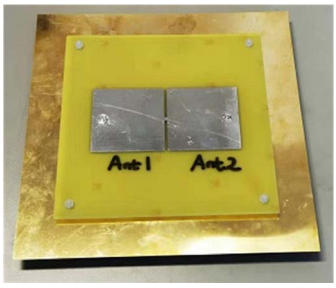

Fig. 14. Photograph of the extremely closely spaced patch antennas with a center connecting strip for decoupling.

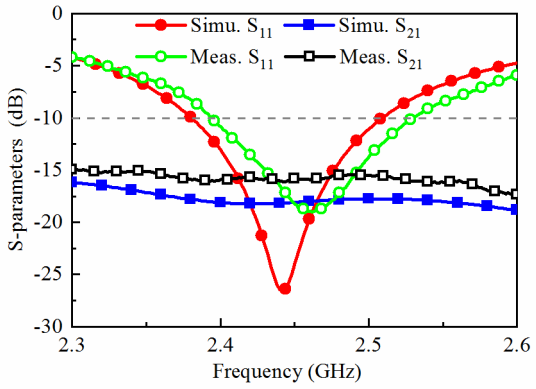

Fig. 15. Simulated and measured S_{11} and S_{21} of the proposed extremely closely spaced patch antennas.

When Ws = 3.2 mm, a good −10 dB impedance bandwidth from 2.38 to 2.51 GHz (5.3%) and an optimized isolation of better than 17.7 dB is realized.

C. Antenna Fabrication

In order to validate the feasibility of the proposed antenna model, a prototype is fabricated as shown in Fig. 14. The patch elements and center decoupling strip are printed on a 1 mm thick FR-4 substrate by the standard printed circuit board process. The patch elements are fed by copper probes. The bottom ground plane is manufactured by a 0.5 mm thick brass ($\sigma = 1.5 \times 10^7$ S/m) plate with the laser cutting process. The FR-4 substrate and ground plane are fixed by four nylon pillars with an air gap of 5 mm.

D. Measured Results

Fig. 15 shows the simulated and measured S_{11} and S_{21} of the proposed extremely closely spaced patch antennas. Due to the structure symmetry, the reflection coefficient of element 2

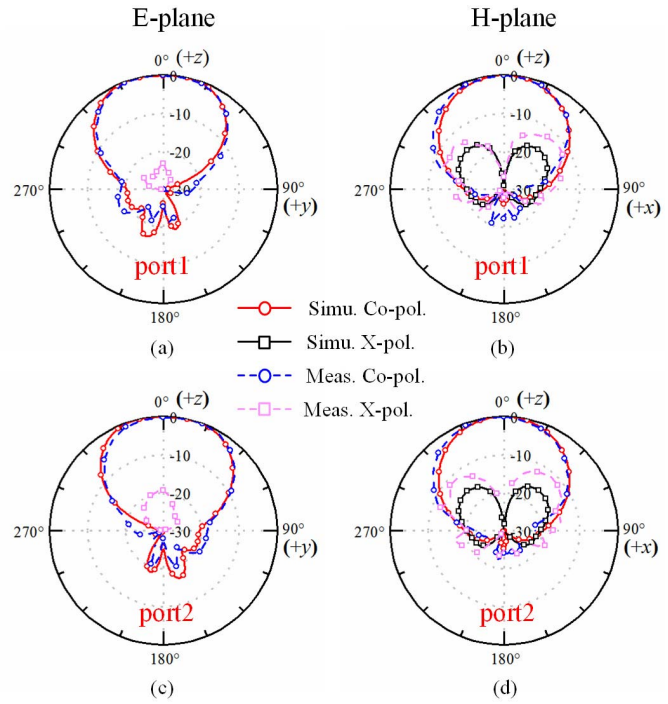

Fig. 16. Simulated and measured normalized radiation pattern of the proposed extremely closely spaced patch antennas at 2.45 GHz on (a) E-plane when fed through port1 and (b) port2, and (c) H-plane when fed through port1 and (d) port2.

is same with that of element 1, which is not shown for brevity. The measured results are in line with the simulated results. The simulated −10 dB S_{11} bandwidth is 2.380–2.510 GHz (5.3%), whereas the measured result is 2.394–2.530 GHz (5.5%) with a center operating frequency of 2.46 GHz. The small frequency deviation is caused by the manual error of the height of the air gap. The simulated isolation is better than 17.7 dB, whereas the measured isolation is better than 15.4 dB across the entire matched bandwidth. The slight isolation deterioration is caused by the fabrication error.

The simulated and measured normalized radiation patterns of the decoupled patch antenna elements at 2.45 GHz are shown in Fig. 16. In the E-plane, the radiation pattern exhibits a slight asymmetric shape for both antenna elements because the adjacent patch element has a little parasitic effect to the driven patch element. Nevertheless, a high measured FBR of 25 dB and a low cross-polarization of less than −23 dB are realized. In the H-plane, the radiation pattern is symmetric and same for both antenna elements. The measured FBR is 25 dB and cross-polarization is less than −11 dB in the H-plane. The conical-like cross-polarization is caused by the radiation of feeding probes.

Fig. 17 presents the simulated and measured antenna efficiency and broadside gain for the decoupled patch elements. The measured results are in a good agreement with the simulated results. The simulated radiation efficiencies of the decoupled antenna and isolated antenna are both presented for comparison. The radiation efficiency of the isolated antenna is better than 96.7% due to the low metallic and dielectric loss. And the radiation efficiency of the decoupled antenna is also better than 93.1%. The simulated total antenna efficiency is

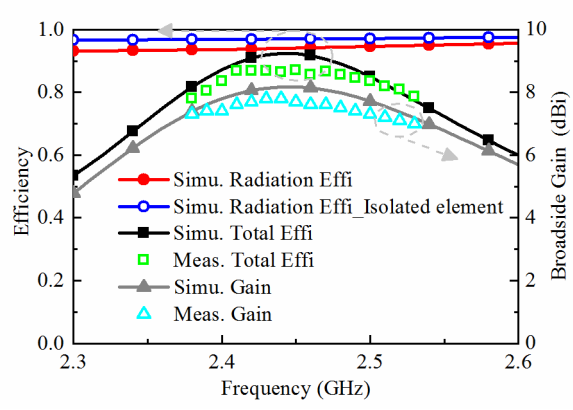

Fig. 17. Simulated and measured antenna efficiency and broadside gain for the extremely closely spaced patch antennas.

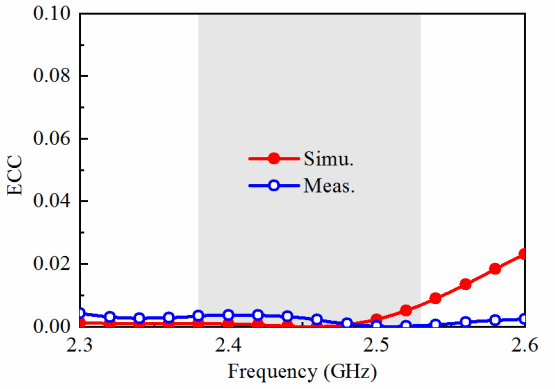

Fig. 18. Simulated and measured ECCs between two extremely closely spaced patch antennas.

from 81.7% to 92.5% across the operating bandwidth, whereas the measured result is from 81.9% to 87.0%. The simulated broadside gain is 7.4–8.2 dBi, whereas the measured broadside gain is 7.0–7.8 dBi across the operating bandwidth.

To evaluate the diversity performance of the proposed extremely closely spaced antenna system, the simulated and measured envelope correlation coefficients (ECCs) are shown in Fig. 18. Note that the ECCs are calculated by the simulated and measured far fields. As seen, an excellent diversity performance with simulated ECC $<$ 0.007 and measured ECC $<$ 0.004 is realized in the desired band.

E. Comparison

To highlight the merits of the proposed decoupling scheme, Table I compares our decoupling scheme with other decoupling methods for closely spaced patch antennas. As seen, compared to decoupling network, EBG, DGS, and parasitic elements, our decoupling scheme has a simpler structure with a tiny footprint. Moreover, the proposed decoupling scheme has the ability to reduce the mutual coupling from a strong coupling status, while other decoupling methods [10], [13], [16], [19], [30] mainly focus on decoupling from a weak coupling ($S_{21} < -10$ dB) to a perfect isolation ($S_{21} < -30$ dB). The combined decoupling method in [34] with isolated wall and parasitic elements has a promising strong-coupling suppression, but

TABLE I

COMPARISONS OF THE DECOUPLING PERFORMANCE BETWEEN CLOSELY SPACED PATCH ANTENNAS

Ref.	Decoupling Schemes	Structure Complexity	Array Config.	Edge-to-edge/ center-to-center distance	Profile	BW	Isolation	FBR	Max. Gain
[10]	Decoupling network	complex	E-plane	0.345 λ_0/0.65 λ_0	0.2 λ_0	5.3%	>28 dB	~15 dB	6.5 dB
[13]	EBG	complex	E-plane	NG / 0.50 λ_0	0.049 λ_0	1.7%	>20 dB	–	–
[16]	SRR DGS	complex	E-plane	0.039 λ_0/0.27 λ_0	0.017 λ_0	1.5%	>56 dB	8.3 dB	3.7 dBi
[19]	DGS	moderate	E-plane	0.031 λ_0/0.33 λ_0	–	1.7%	>40 dB	~3 dB	~0.5 dBi
[30]	Parasitic elements	moderate	H-plane	0.29 λ_0/0.60 λ_0	0.077 λ_0	4.9%	>30 dB	~18 dB	~7.7 dBi
[34]	Isolated wall+ Parasitic elements	complex	H-plane	0.03 λ_0/0.28 λ_0	0.22 λ_0	1.4%	>35 dB	~15 dB	–
Proposed	Inductance	simple	E-plane	0.016 λ_0/0.44 λ_0	0.049 λ_0	5.5%	>15.4 dB	25 dB	7.8 dBi

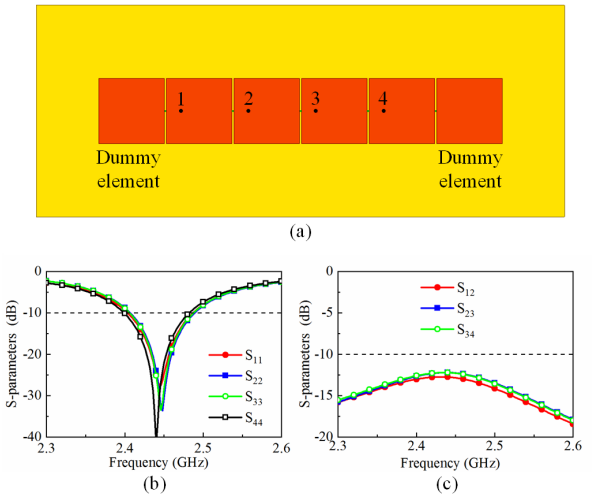

Fig. 19. (a) Configuration of the extremely closely spaced 1 × 4 patch array with two side dummy elements. (b) Simulated reflection coefficients. (c) Simulated transmission coefficients.

suffers from a large decoupling structure with an increased profile of 0.22 λ_0. Habashi *et al.* [16] and Ouyang *et al.* [19] can reduce the mutual coupling between closely spaced patch antennas with E-plane array configuration by the DGS method, but the decoupling bandwidths are limited to less than 2% and the radiation patterns are severely influenced by the decoupling structure with a low FBR and antenna gain. In summary, compared to the previous decoupling approaches, our decoupling scheme has the merits of simple structure, tiny occupied dimension, strong-coupling suppression ability, low profile, moderate bandwidth, and improved radiation pattern with a high FBR and antenna gain. The limitation of the proposed decoupling scheme is that it is competent for the strong-coupling reduction but incompetent for the weak-coupling reduction. That is, the decoupling performance will be deteriorated gradually with the increase of the element distance.

IV. EXTENSION TO 1-D AND 2-D LARGE ARRAYS

To validate the feasibility of the proposed decoupling scheme for practical large-scale array applications, such as the closely spaced phased array or massive MIMO array, the simulated results of 1-D and 2-D arrays are discussed in this section.

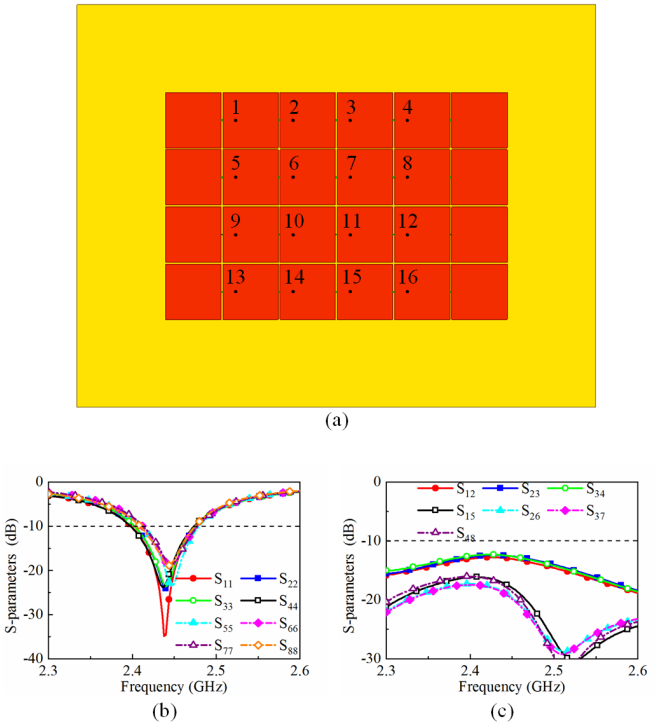

Fig. 20. (a) Configuration of the closely spaced 4 × 4 patch array with two columns of dummy elements. (b) Simulated reflection coefficients. (c) Simulated transmission coefficients.

A. 1-D Array

Fig. 19(a) shows the array model of the proposed extremely closely spaced 1 × 4 patch array. Note that the patch element is installed in the air medium with a low profile of 5 mm above a 200 × 500 mm^2 ground plane. The edge-to-edge distance between adjacent elements is only 2 mm. Two dummy elements are placed at both sides of the array to balance the impedance for all elements. With the strong mutual coupling effect between adjacent elements, the impedance matching

and isolations are severely deteriorated for all elements. By inserting an optimized 1 nH inductance between each group of adjacent elements, a good mutual coupling reduction performance is realized as shown in Fig. 19(b) and (c). As seen, the impedance matching is improved for all elements with a −10 dB bandwidth of 85 MHz. The isolations between adjacent elements have been improved from 5 dB to better than 12.2 dB with a strong coupling reduction. The isolations between non-adjacent elements are all better than 20 dB, which is not shown for brevity. Note that the impedance bandwidth and isolations of four-element array are slightly deteriorated compared to the two-element array due to the influence of the closely spaced configuration at both sides of the patch element and the imperfect symmetry of dummy elements.

B. 2-D Array

With the weak coupling effect between extremely closely spaced H-plane arrayed patch antennas as early proposed in Fig. 1(d)–(f), the 1-D array can be readily extended to a 2-D array as shown in Fig. 20(a). The element dimensions and distance of the 2-D array are same with those in the 1-D array. Also, two columns of dummy elements are placed at both sides of the 2-D array. In E-plane, 20 lumped inductances, with an optimized value of L = 1.2 nH, are inserted between adjacent elements for the coupling reduction. In H-plane, no decoupling components are needed. The simulated S-parameters of the 4 × 4 array are presented in Fig. 20(b) and (c). As seen, the −10 dB impedance bandwidth is 70 MHz. The isolations between adjacent elements in E-plane are improved to better than 12.0 dB, while the isolations between adjacent elements in H-plane are better than 16.0 dB.

V. Conclusion

In this article, a simple and effective decoupling scheme is proposed to reduce the strong mutual coupling between extremely closely spaced patch antennas by inserting a lumped inductance or an inductive connecting strip. A systemic design guideline, based on the MCM, is proposed to explain the decoupling mechanism. Then, a prototype is simulated, fabricated, and measured to validate the proposed decoupling concept. The measured results show that the proposed decoupling scheme can improve the antenna isolation from 5 dB to better than 15.4 dB across the matched bandwidth of 2.394–2.530 GHz (5.5%), with an extremely close edge-to-edge distance of 0.016 λ_0 and a center-to-center distance of 0.44 λ_0. At the same time, the radiation pattern is also improved with a high FBR of 25 dB and a broadside gain of 7.8 dBi. The measured antenna efficiency is from 81.9% to 87.0% and the measured ECC is less than 0.004 across the matched bandwidth, which indicates a good radiation and diversity performance. Furthermore, the validation of extending to large-scale 1-D and 2-D arrays is also discussed. To the best of the authors' knowledge, it is the simplest decoupling scheme in the open literature to suppress the strong coupling between extremely closely spaced patch antennas, which is a promising candidate for the closely spaced MIMO antennas and phased array applications.

References

[1] J. Winters, "On the capacity of radio communication systems with diversity in a Rayleigh fading environment," *IEEE J. Sel. Areas Commun.*, vol. SAC-5, no. 5, pp. 871–878, Jun. 1987.

[2] M. A. Jensen and J. W. Wallace, "A review of antennas and propagation for MIMO wireless communications," *IEEE Trans. Antennas Propag.*, vol. 52, no. 11, pp. 2810–2824, Nov. 2004.

[3] Z. Zhang, *Antenna Design for Mobile Devices*, 2nd ed. Hoboken, NJ, USA: Wiley, 2017.

[4] X. Chen, S. Zhang, and Q. Li, "A review of mutual coupling in MIMO systems," *IEEE Access*, vol. 6, pp. 24706–24719, 2018.

[5] H. Li and B. K. Lau, "MIMO systems and antennas for terminals," in *Handbook of Antenna Technologies*, Z. N. Chen, D. Liu, H. Nakano, X. Qing, and T. Zwick, Eds. Singapore: Springer, 2016.

[6] S.-C. Chen, Y.-S. Wang, and S.-J. Chung, "A decoupling technique for increasing the port isolation between two strongly coupled antennas," *IEEE Trans. Antennas Propag.*, vol. 56, no. 12, pp. 3650–3658, Dec. 2008.

[7] X. Tang, K. Mouthaan, and J. C. Coetzee, "Tunable decoupling and matching network for diversity enhancement of closely spaced antennas," *IEEE Antennas Wireless Propag. Lett.*, vol. 11, pp. 268–271, 2012.

[8] L. Zhao, L. K. Yeung, and K.-L. Wu, "A coupled resonator decoupling network for two-element compact antenna arrays in mobile terminals," *IEEE Trans. Antennas Propag.*, vol. 62, no. 5, pp. 2767–2776, May 2014.

[9] M. Li, L. Jiang, and K. L. Yeung, "Novel and efficient parasitic decoupling network for closely coupled antennas," *IEEE Trans. Antennas Propag.*, vol. 67, no. 6, pp. 3574–3585, Jun. 2019.

[10] R.-L. Xia, S.-W. Qu, P.-F. Li, Q. Jiang, and Z.-P. Nie, "An efficient decoupling feeding network for microstrip antenna array," *IEEE Antennas Wireless Propag. Lett.*, vol. 14, pp. 871–874, 2015.

[11] F. Yang and Y. Rahmat-Samii, "Microstrip antennas integrated with electromagnetic band-gap (EBG) structures: A low mutual coupling design for array applications," *IEEE Trans. Antennas Propag.*, vol. 51, no. 10, pp. 2936–2946, Oct. 2003.

[12] E. Rajo-Iglesias, Ó. Quevedo-Teruel, and L. Inclan-Sanchez, "Mutual coupling reduction in patch antenna arrays by using a planar EBG structure and a multilayer dielectric substrate," *IEEE Trans. Antennas Propag.*, vol. 56, no. 6, pp. 1648–1655, Jun. 2008.

[13] H. S. Farahani, M. Veysi, M. Kamyab, and A. Tadjalli, "Mutual coupling reduction in patch antenna arrays using a UC-EBG superstrate," *IEEE Antennas Wireless Propag. Lett.*, vol. 9, pp. 57–59, 2010.

[14] E. Rajo-Iglesias, Ó. Quevedo-Teruel, and L. Imclan-Sanchez, "Planar soft surfaces and their application to mutual coupling reduction," *IEEE Trans. Antennas Propag.*, vol. 57, no. 12, pp. 2859–3852, Dec. 2009.

[15] C.-Y. Chiu, C.-H. Cheng, R. D. Murch, and C. R. Rowell, "Reduction of mutual coupling between closely-packed antenna elements," *IEEE Trans. Antennas Propag.*, vol. 55, no. 6, pp. 1732–1738, Jun. 2007.

[16] A. Habashi, J. Nourinia, and C. Ghobadi, "Mutual coupling reduction between very closely spaced patch antennas using low-profile folded split-ring resonators (FSRRs)," *IEEE Antennas Wireless Propag. Lett.*, vol. 10, pp. 862–865, 2011.

[17] S. Zhang, S. N. Khan, and S. He, "Reducing mutual coupling for an extremely closely-packed tunable dual-element PIFA array through a resonant slot antenna formed in-between," *IEEE Trans. Antennas Propag.*, vol. 58, no. 8, pp. 2771–2776, Aug. 2010.

[18] S. Zhang, B. K. Lau, Y. Tan, Z. Ying, and S. He, "Mutual coupling reduction of two PIFAs with a T-shape slot impedance transformer for MIMO mobile terminals," *IEEE Trans. Antennas Propag.*, vol. 60, no. 3, pp. 1521–1531, Mar. 2012.

[19] J. OuYang, F. Yang, and Z. M. Wang, "Reducing mutual coupling of closely spaced microstrip MIMO antennas for WLAN application," *IEEE Antennas Wireless Propag. Lett.*, vol. 10, pp. 310–313, 2011.

[20] J. Ghosh, D. Mitra, and S. Das, "Mutual coupling reduction of slot antenna array by controlling surface wave propagation," *IEEE Trans. Antennas Propag.*, vol. 67, no. 2, pp. 1352–1357, Feb. 2019.

[21] A. Diallo, C. Luxey, P. Le Thuc, R. Staraj, and G. Kossiavas, "Study and reduction of the mutual coupling between two mobile phone PIFAs operating in the DCS1800 and UMTS bands," *IEEE Trans. Antennas Propag.*, vol. 54, no. 11, pp. 3063–3074, Nov. 2006.

[22] A. Diallo, P. Le Thuc, R. Staraj, G. Kossiavas, and C. Luxey, "Enhanced two-antenna structures for universal mobile telecommunications system diversity terminals," *IET Microw., Antennas Propag.*, vol. 2, no. 1, pp. 93–101, Feb. 2008.

[23] S. Ranvier *et al.*, "Mutual coupling reduction for patch antenna array," in *Proc. 1st Eur. Conf. Antennas Propag. (EuCAP)*, Nov. 2006.

[24] Y. Wang and Z. Du, "A wideband printed dual-antenna system with a novel neutralization line for mobile terminals," *IEEE Antennas Wireless Propag. Lett.*, vol. 12, pp. 1428–1431, Oct. 2013.
[25] Y. Wang and Z. Du, "A wideband printed dual-antenna with three neutralization lines for mobile terminals," *IEEE Trans. Antennas Propag.*, vol. 62, no. 3, pp. 1495–1500, Mar. 2014.
[26] K.-L. Wong, J.-Y. Lu, L.-Y. Chen, W.-Y. Li, and Y.-L. Ban, "8-antenna and 16-antenna arrays using the quad-antenna linear array as a building block for the 3.5-GHz LTE MIMO operation in the smartphone," *Microw. Opt. Technol. Lett.*, vol. 58, no. 1, pp. 174–181, Jan. 2016.
[27] D. N. P. Thalakotuna, Z. Hu, and J. B. Beresford, "Reflection cancellation in multibeam antennas," U.S. Patent 14 596 939, Jan. 14, 2015.
[28] A. C. K. Mak, C. R. Rowell, and R. D. Murch, "Isolation enhancement between two closely packed antennas," *IEEE Trans. Antennas Propag.*, vol. 56, no. 11, pp. 3411–3419, Nov. 2008.
[29] B. K. Lau and J. B. Andersen, "Simple and efficient decoupling of compact arrays with parasitic scatterers," *IEEE Trans. Antennas Propag.*, vol. 60, no. 2, pp. 464–472, Feb. 2012.
[30] S. Farsi, H. Aliakbarian, D. Schreurs, B. Nauwelaers, and G. A. E. Vandenbosch, "Mutual coupling reduction between planar antennas by using a simple microstrip U-section," *IEEE Antennas Wireless Propag. Lett.*, vol. 11, pp. 1501–1503, 2012.
[31] L. Zhao and K.-L. Wu, "A decoupling technique for four-element symmetric arrays with reactively loaded dummy elements," *IEEE Trans. Antennas Propag.*, vol. 62, no. 8, pp. 4416–4421, Aug. 2014.
[32] S. Hong, K. Chung, J. Lee, S. Jung, S.-S. Lee, and J. Choi, "Design of a diversity antenna with stubs for UWB applications," *Microw. Opt. Technol. Lett.*, vol. 50, no. 5, pp. 1352–1356, 2008.
[33] H. Wang, L. Liu, Z. Zhang, Y. Li, and Z. Feng, "A wideband compact WLAN/WiMAX MIMO antenna based on dipole with V-shaped ground branch," *IEEE Trans. Antennas Propag.*, vol. 63, no. 5, pp. 2290–2295, May 2015.
[34] H. Qi, L. Liu, X. Yin, H. Zhao, and W. J. Kulesza, "Mutual coupling suppression between two closely spaced microstrip antennas with an asymmetrical coplanar strip wall," *IEEE Antennas Wireless Propag. Lett.*, vol. 15, pp. 191–194, 2016.
[35] M.-C. Tang *et al.*, "Mutual coupling reduction using meta-structures for wideband, dual-polarized, and high-density patch arrays," *IEEE Trans. Antennas Propag.*, vol. 65, no. 8, pp. 3986–3998, Aug. 2017.
[36] J. Zhu and G. V. Eleftheriades, "A simple approach for reducing mutual coupling in two closely spaced metamaterial-inspired monopole antennas," *IEEE Antennas Wireless Propag. Lett.*, vol. 9, pp. 379–382, 2010.
[37] K.-L. Wong, C.-Y. Tsai, and J.-Y. Lu, "Two asymmetrically mirrored gap-coupled loop antennas as a compact building block for eight-antenna MIMO array in the future smartphone," *IEEE Trans. Antennas Propag.*, vol. 65, no. 4, pp. 1765–1778, Apr. 2017.
[38] D. R. Hendry and A. M. Abbosh, "Coupled-resonator theory of isolation in multi-mode antennas," *IEEE Trans. Antennas Propag.*, vol. 67, no. 9, pp. 5801–5811, Sep. 2019.
[39] L. Sun, Y. Li, Z. Zhang, and H. Wang, "Self-decoupled MIMO antenna pair with shared radiator for 5G smartphones," *IEEE Trans. Antennas Propag.*, vol. 68, no. 5, pp. 3423–3432, May 2020.
[40] D. M. Pozar, *Microwave Engineering*, 2nd ed. New York, NY, USA: Wiley, 1998.
[41] D. E. Bockelman and W. R. Eisenstadt, "Combined differential and common-mode scattering parameters: Theory and simulation," *IEEE Trans. Microw. Theory Techn.*, vol. 43, no. 7, pp. 1530–1539, Jul. 1995.
[42] R. Garg and I. J. Bahl, "Characteristics of coupled microstriplines," *IEEE Trans. Microw. Theory Techn.*, vol. MTT-27, no. 7, pp. 700–705, Jul. 1979.

Libin Sun (Graduate Student Member, IEEE) received the B.S. degree from Xidian University, Xi'an, China, in 2016. He is currently pursuing the Ph.D. degree with the Department of Electrical and Engineering, Tsinghua University, Beijing, China.

He has authored over ten journal articles and holds five granted Chinese patents. His current research interests include antenna design and theory, particularly in 5G mobile phone antennas, antenna decoupling, MIMO and diversity antennas, circularly polarized antennas, leaky-wave antennas, and surface-wave antennas.

Mr. Sun was a recipient of the Top Reviewer Award of the IEEE TRANSACTIONS ON ANTENNAS AND PROPAGATION in 2019 and the Honorable Mention in the 2020 IEEE AP-S Student Paper Competition. He serves as a Reviewer for several international academic journals, such as the IEEE TRANSACTIONS ON ANTENNAS AND PROPAGATION, the IEEE ANTENNAS AND WIRELESS PROPAGATION LETTERS, IEEE ACCESS, the *IET Microwaves, Antennas and Propagation*, the *IET Electronics Letters*, and *Microwave and Optical Technology Letters*.

Yue Li (Senior Member, IEEE) received the B.S. degree in telecommunication engineering from Zhejiang University, Zhejiang, China, in 2007, and the Ph.D. degree in electronic engineering from Tsinghua University, Beijing, China, in 2012.

In June 2012, he was a Post-Doctoral Fellow with the Department of Electronic Engineering, Tsinghua University, where he is currently an Associate Professor with the Department of Electronic Engineering. In December 2013, he was a Research Scholar with the Department of Electrical and Systems Engineering, University of Pennsylvania, Philadelphia, PA, USA. He was also a Visiting Scholar with the Institute for Infocomm Research (I2R), A∗STAR, Singapore, in 2010, and the Hawaii Center of Advanced Communication (HCAC), University of Hawaii at Manoa, Honolulu, HI, USA, in 2012. Since January 2016, he has been with Tsinghua University, where he is currently an Assistant Professor. He has authored or coauthored over 150 journal articles and 45 international conference papers, and he holds 20 granted Chinese patents. His current research interests include metamaterials, plasmonics, electromagnetics, nanocircuits, mobile and handset antennas, MIMO and diversity antennas, and millimeter-wave antennas and arrays.

Dr. Li was a recipient of the Issac Koga Gold Medal from the URSI General Assembly in 2017, the Second Prize of Science and Technology Award of the China Institute of Communications in 2017, the Young Scientist Awards from the conferences of PIERS 2019, ACES 2018, AT-RASC 2018, AP-RASC 2016, EMTS 2016, and URSI GASS 2014, the Best Paper Awards from the conferences of APCAP 2020/2017, UCMMT 2020, ISAP 2019, CSQRWC 2018, ISAPE 2016, and ICMMT 2020/2016, the Outstanding Doctoral Dissertation of Beijing Municipality in 2013, and the Principal Scholarship of Tsinghua University in 2011. He serves as an Associate Editor for the IEEE TRANSACTIONS ON ANTENNAS AND PROPAGATION, the IEEE ANTENNAS AND WIRELESS PROPAGATION LETTERS, *Microwave and Optical Technology Letters*, and *Computer Applications in Engineering Education*, and also as the Editorial Board Member of *Scientific Report*.

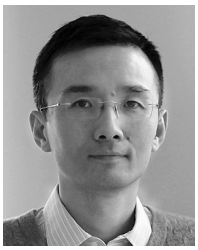

Zhijun Zhang (Fellow, IEEE) received the B.S. and M.S. degrees from the University of Electronic Science and Technology of China, Chengdu, China, in 1992 and 1995, respectively, and the Ph.D. degree from Tsinghua University, Beijing, China, in 1999.

In 1999, he was a Post-Doctoral Fellow with the Department of Electrical Engineering, The University of Utah, Salt Lake City, UT, USA, where he was appointed a Research Assistant Professor in 2001. In May 2002, he was an Assistant Researcher with the University of Hawaii at Manoa, Honolulu, HI, USA. In November 2002, he joined Amphenol T&M Antennas, Vernon Hills, IL, USA, as a Senior Staff Antenna Development Engineer and was then promoted to the position of Antenna Engineer Manager. In 2004, he joined Nokia Inc., San Diego, CA, USA, as a Senior Antenna Design Engineer. In 2006, he joined Apple Inc., Cupertino, CA, USA, as a Senior Antenna Design Engineer and was then promoted to the position of Principal Antenna Engineer. Since August 2007, he has been with Tsinghua University, where he is currently a Professor with the Department of Electronic Engineering. He is the author of *Antenna Design for Mobile Devices* (Wiley, First Edition 2011, Second Edition 2017).

Dr. Zhang has served as an Associate Editor for the IEEE TRANSACTIONS ON ANTENNAS AND PROPAGATION from 2010 to 2014 and the IEEE ANTENNAS AND WIRELESS PROPAGATION LETTERS from 2009 to 2015.